Novel Approach to Prompt Fission Neutron Investigation

Sh. Zeynalov, O. Zeynalova, P.Sedyshev, V. Shvetsov

JINR-Joint Institute for Nuclear Research, Dubna, Russia

Motivation

Scission neutrons were predicted in 1939 in classic paper of N. Bohr and J. Wheeler. First experiments made in 1960-ies by Manhattan Group concluded existence of scission neutrons for ^{252}Cf(sf). Soon after scission neutrons were discovered for ^{235}U(n,f) by K. Skarsvag and I. Singstad.

C. Budtz-Jǿrgensen and H.-H. Knitter investigated ^{252}Cf(sf) in simultaneous measurement of FF, kinetic energies, mass and the FF emission angle. Less than<1% of scission neutrons was concluded from the PFN angular distribution analysis in FF centre-of-mass reference system in that work. According to the theory models linear dependence of average PFN multiplicity on TKE in fission is expected, but the experiment did not confirm that.

The results obtained using DPP for PFN investigation in ^{252}Cf(sf) reaction in EC-JRC-IRMM during 2005-2007 for the first time confirm results of C. Budtz-Jǿrgensen and H.-H. Knitter, at the same time revealing linear dependence of PFN number on TKE release in fission. We further developed fission detector and mathematical data analysis, which we believe opens the new perspectives in study nuclei at low excitation energies, undergoing the nuclear superfluid to normal liquid phase transition. The scission configuration offers the unique possibility to investigate, how two different nuclei at constant temperature share the available intrinsic excitation when they are in thermal contact.

Pre-scission nuclear shape parameterization in MM-RNR and PFN emission

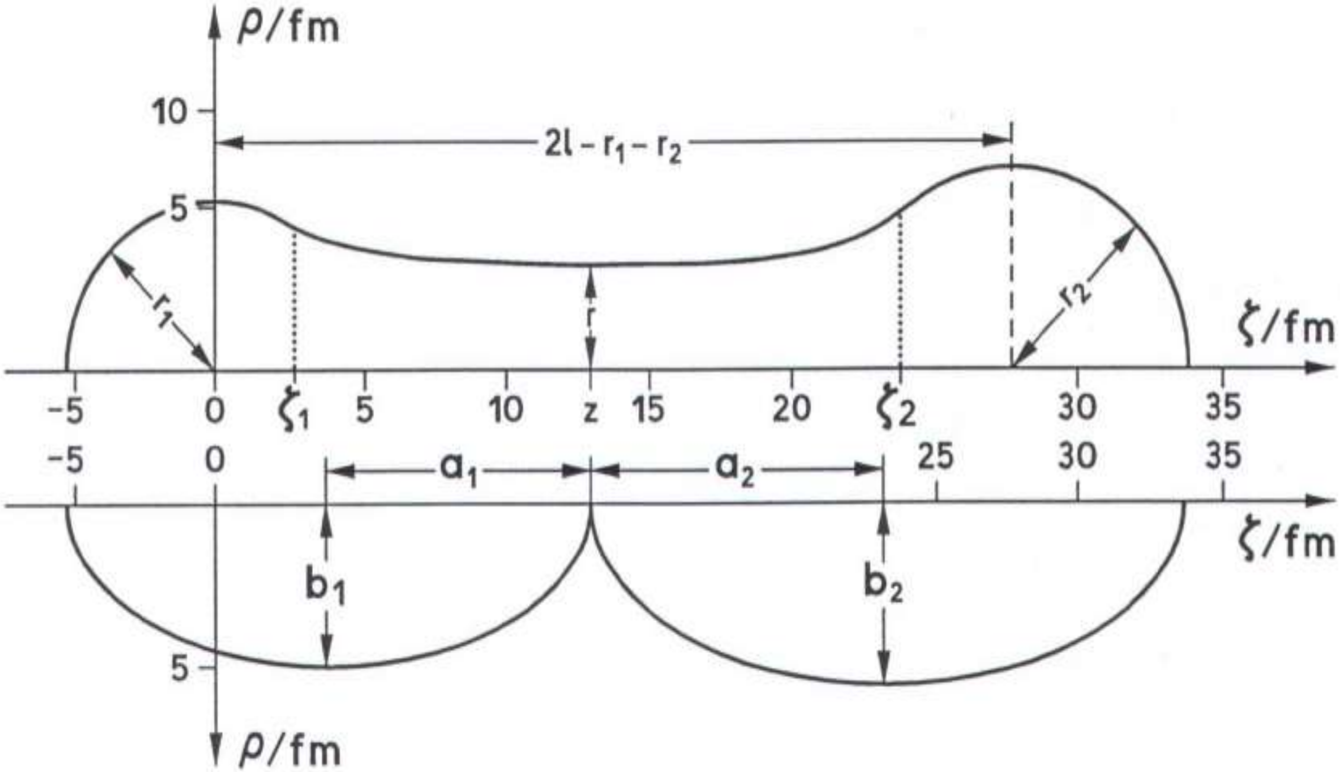

PFN emission mechanism in MM-RNR is considered as RNR, leading to the excited FFs. PFN emission is the first stage of FFs de-excitation, following by γ-ray emission. At scission configuration the temperatures of the nascent fragments remain different in spite of the flow of excitation energy from the hot to cold fragment.

PFN emission kinematics

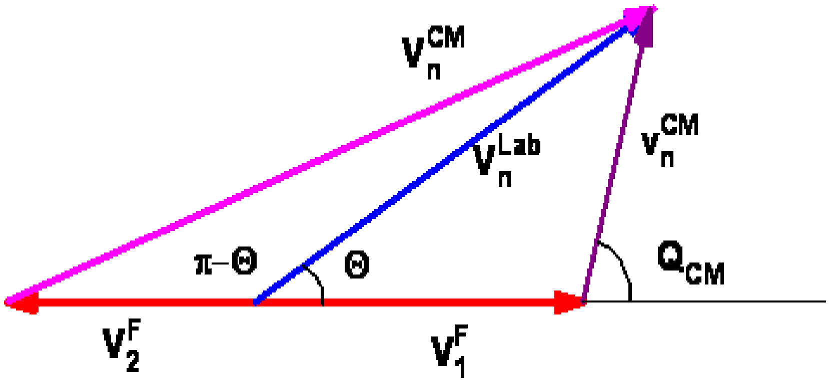

The detailed information on the intrinsic state of the fragments can be obtained by measurement of dependence of the average number of PFN emitted by the FF with mass number A and TKE release of two fission fragments. To do this one needs reconstruction of PFN emission kinematics as illustrated in the figure above.

$$\bar{\nu}(A) = \frac{\int_0^\infty \bar{\nu}(A,TKE)Y(A,TKE)dTKE}{\int_0^\infty Y(A,TKE)dTKE} \text{ or } \bar{\nu}(TKE) = \frac{\int_0^\infty \bar{\nu}(A,TKE)Y(A,TKE)dA}{\int_0^\infty Y(A,TKE)dA}$$

$$\bar{\nu} = \int_0^\infty \bar{\nu}(A,TKE)Y(A,TKE)dTKE\,dA, \quad 200 = \int_0^\infty Y(A,TKE)dTKE\,dA$$

Twin Frisch-grid ionization chamber

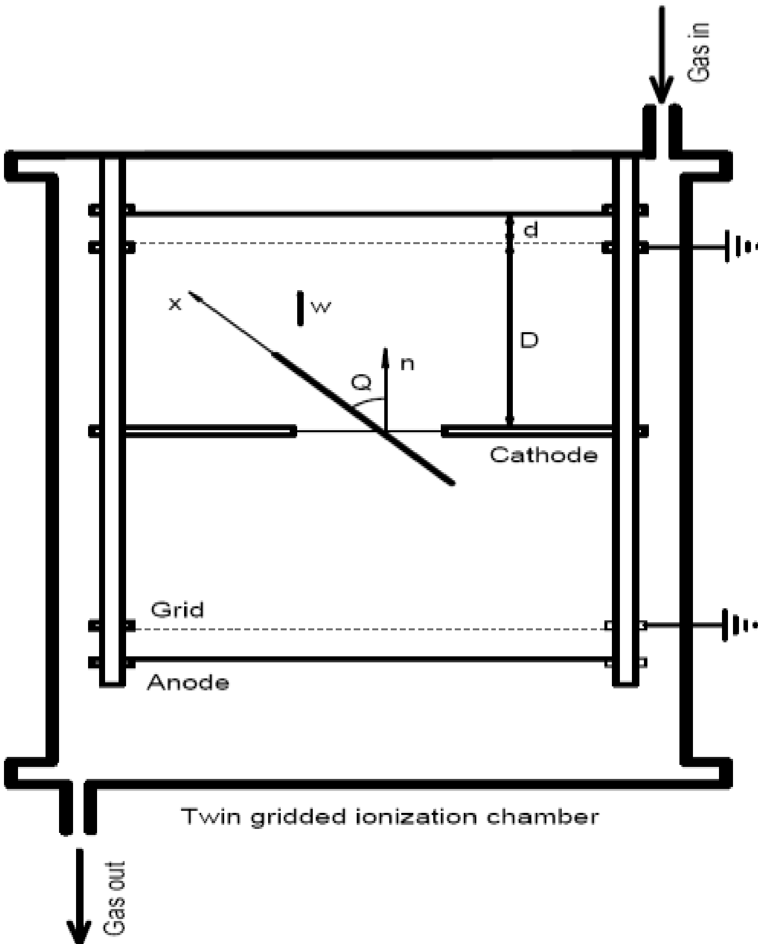

Signals from the TGIC anodes arise because of the motion of charge carriers after they are formed by the FF

The time evolution of the signal is of fundamental importance in understanding the timing proper-ties of pulses as well as in predicting the effects of changes in the location of the radiation interactions on the shape of the pulse.

The Poisson equation is the starting point for these calculations

$$\nabla^2 \varphi = 0, \text{ where } \nabla^2 = \frac{\partial^2}{\partial x^2} + \frac{\partial^2}{\partial y^2}, \quad \text{Electric field } \varepsilon = -grad\, \varphi$$

The Signal Formation

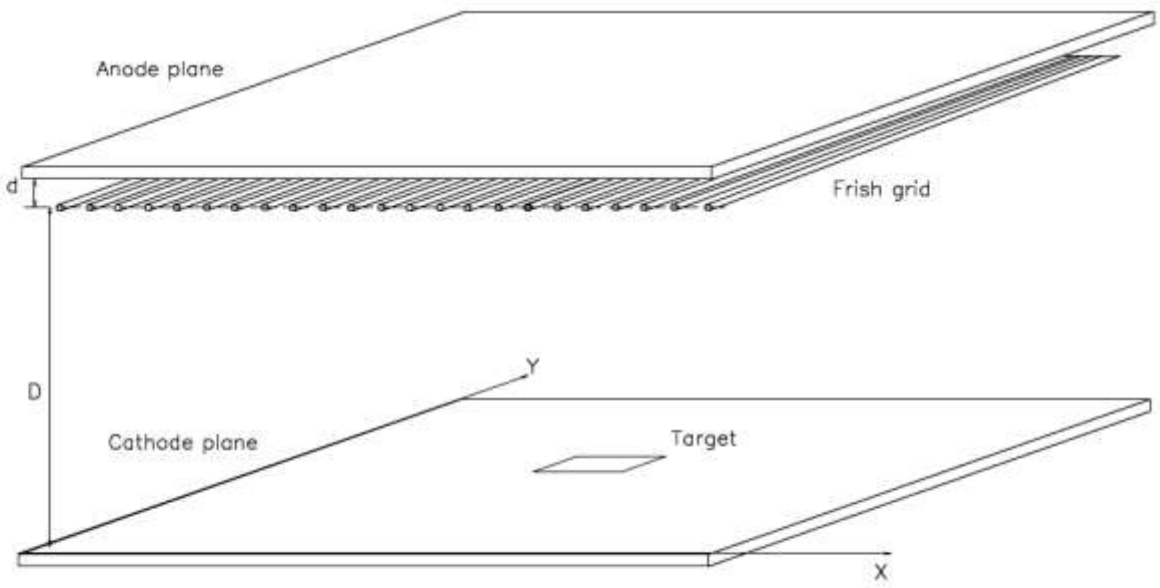

$$Q = q\Delta\varphi_0$$

To find this weighting potential ϕ_0 as a function of position,one must solve the Laplace equation for the geometry of the detector, but with some artificial boundary conditions:

1. **The voltage on the electrode for which the induced charge is to be calculated is set equal to unity.**
2. **The voltages on all other electrodes are set to zero.**
3. **Even if a trapped charge is present within the detector volume, it is ignored in the calculation.**

Finite difference approximation

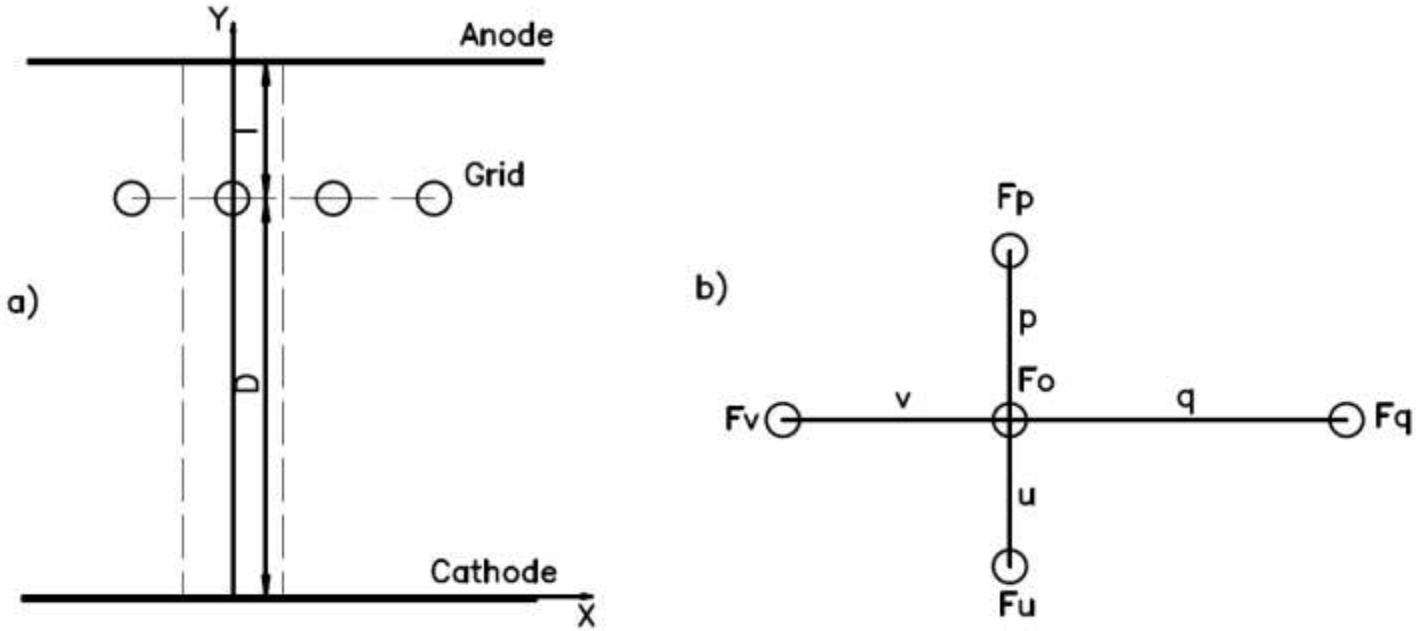

$$\frac{\partial^2 F(x,y)}{\partial x^2} + \frac{\partial^2 F(x,y)}{\partial y^2} = 0$$

$$\frac{\partial^2 F}{\partial x^2} = \frac{2F_v}{v(v+q)} + \frac{2F_q}{q(q+v)} - \frac{2F_o}{qv}, \qquad \frac{\partial^2 F}{\partial y^2} = \frac{2F_p}{p(p+u)} + \frac{2F_u}{u(p+u)} - \frac{2F_o}{pu}$$

$$\frac{F_v}{v(v+q)} + \frac{F_q}{q(v+q)} + \frac{F_p}{p(p+u)} + \frac{F_u}{u(p+u)} = \frac{pu+qv}{puqv} F_o$$ - finite difference Laplace equation

Weighting potential

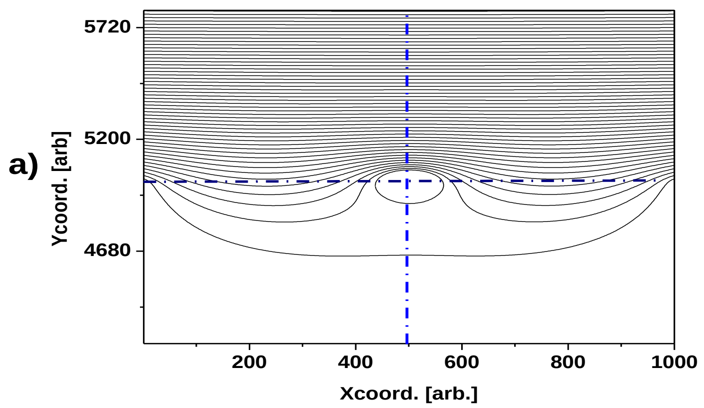

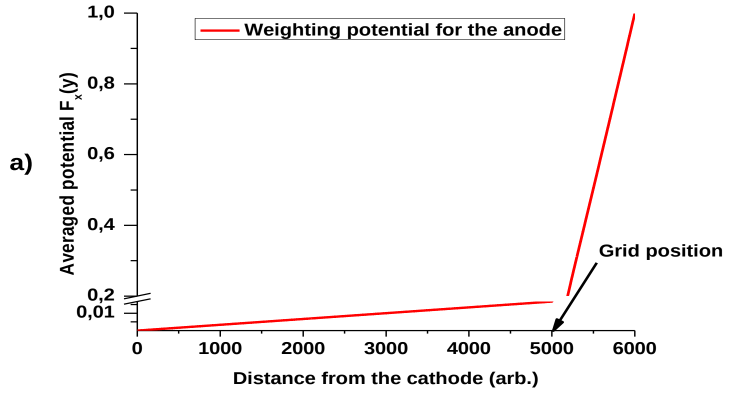

$$Q(y) = (F_x(y) - F_x(y = \tau \times \cos(\Theta)) \times q$$

$$F_x(y) = \begin{cases} \sigma \dfrac{y}{D} \text{ for } 0 \le y < D \\ (1-\sigma)\dfrac{y-D}{l} + \sigma \text{ for } D \le y \le D + l \end{cases}$$

$$dQ(y) = ((1-\sigma) \times \frac{y-D}{l} + \sigma - \sigma \times \frac{\tau \times \cos(\Theta)}{D})\rho(\tau)d\tau$$

$$Q(E, D+d) = \int_0^L e \times \rho(E,\tau) \times (1 - \sigma \times \frac{\tau \times \cos(\Theta)}{D})d\tau = N(E) \times e \times (1 - \sigma\frac{\hat{X}(E) \times \cos(\Theta)}{D})$$

$$T(Q, \cos(\Theta)) = \frac{D}{W}(1 + \frac{l}{2D} - \frac{\overline{X}(Q)}{D}\cos(\Theta))$$

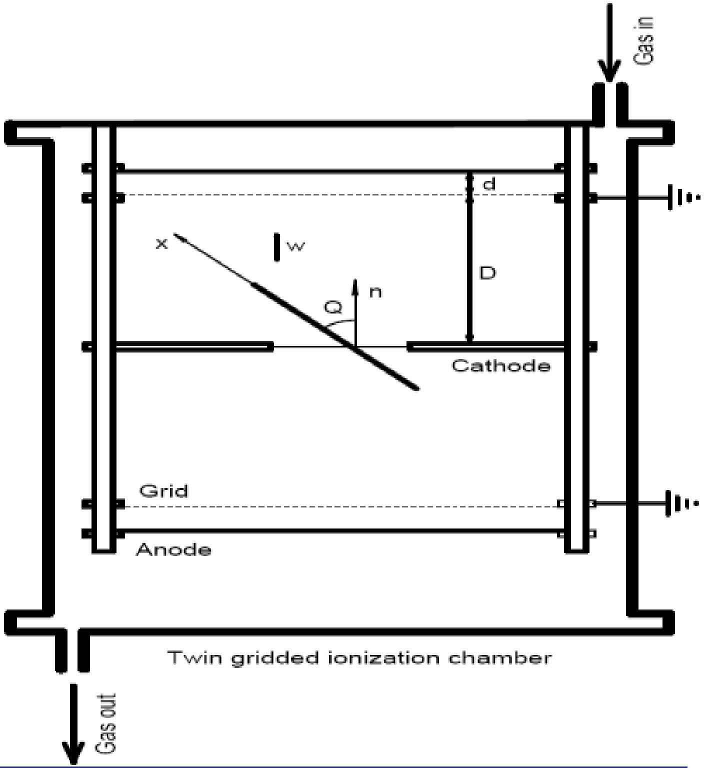

Experimental setup for PFN investigation

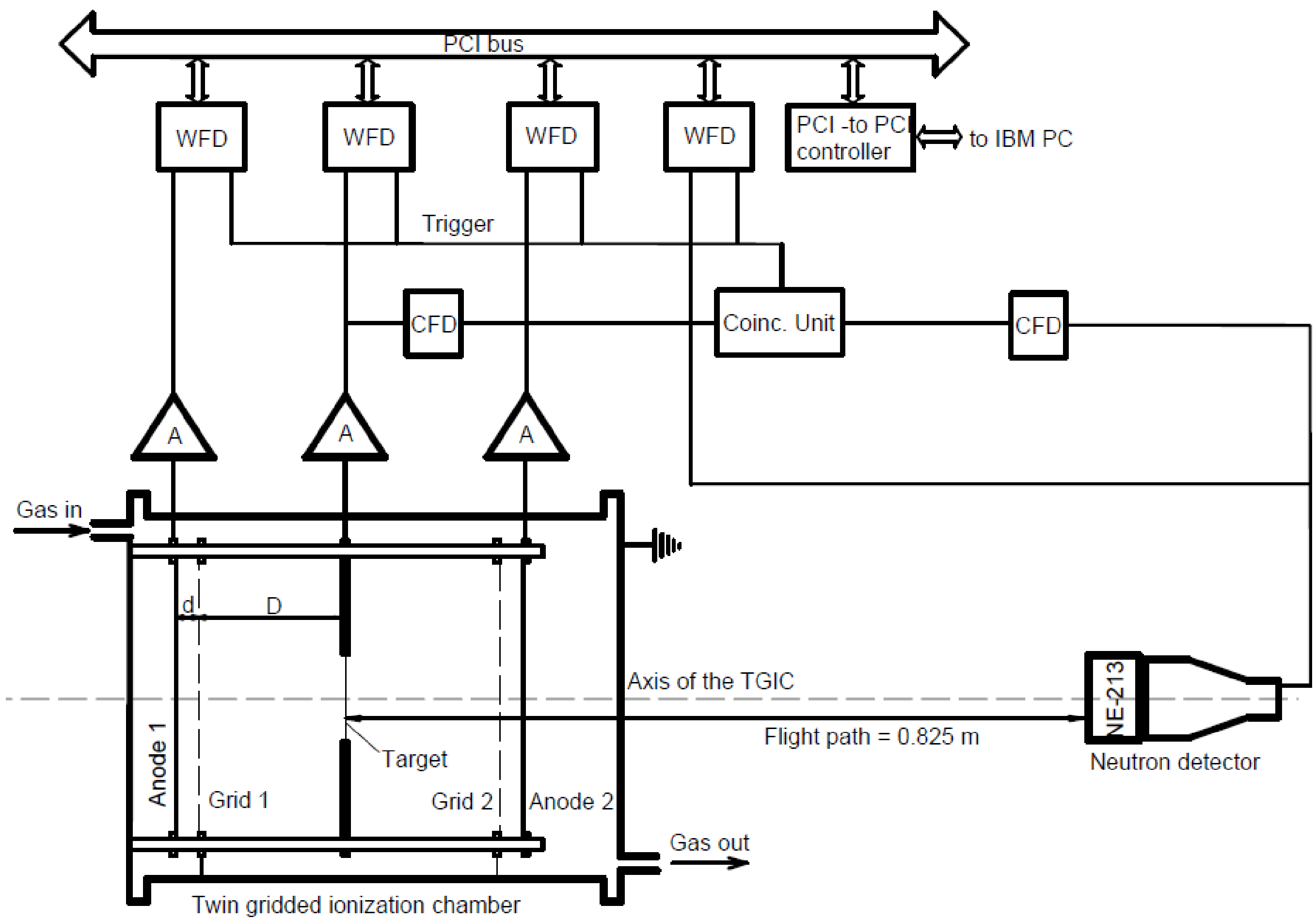

Digital pulse processing steps

Signal processing applied to recorded waveforms (A1, A2, C, N) :

1) FF pulse heights P_1, P_2 calculated as $P_k = \sum_{Tg}^{Tg+N} I_k(i)$ after converting A1, A2 into I1, I2 using unfolding of the following equation: $A_k(t) = \int_0^t I_k(\xi) d\xi$
2) FF drift time T1, T2 calculated $T_{1,2} = \sum_{k=N}^{N+M} k * I[k]$
3) Using relation $T_0 - T(E) = (T_0 - T_{90}(E)) * COS(\Theta)$ between drift time and the Θ (angle between fission axis an the normal to the cathode plane), COS(Θ) was parameterized.
4) FFs kinetic energies were corrected due to losses in the target layer and the target backing.
5) FFs masses and kinetic energies were evaluated in iterative procedure taking into account prompt fission neutron (PFN) emission and its multiplicity dependence on FF mass.
6) Cathode and ND signal waveforms C, N provided the information on the time instant of the fission event and the PFN time-of-flight values, measured using digital constant fraction time marking method. The pulse shape analysis was used to separate PFN from a gamma background.

Real measurement of angular distribution

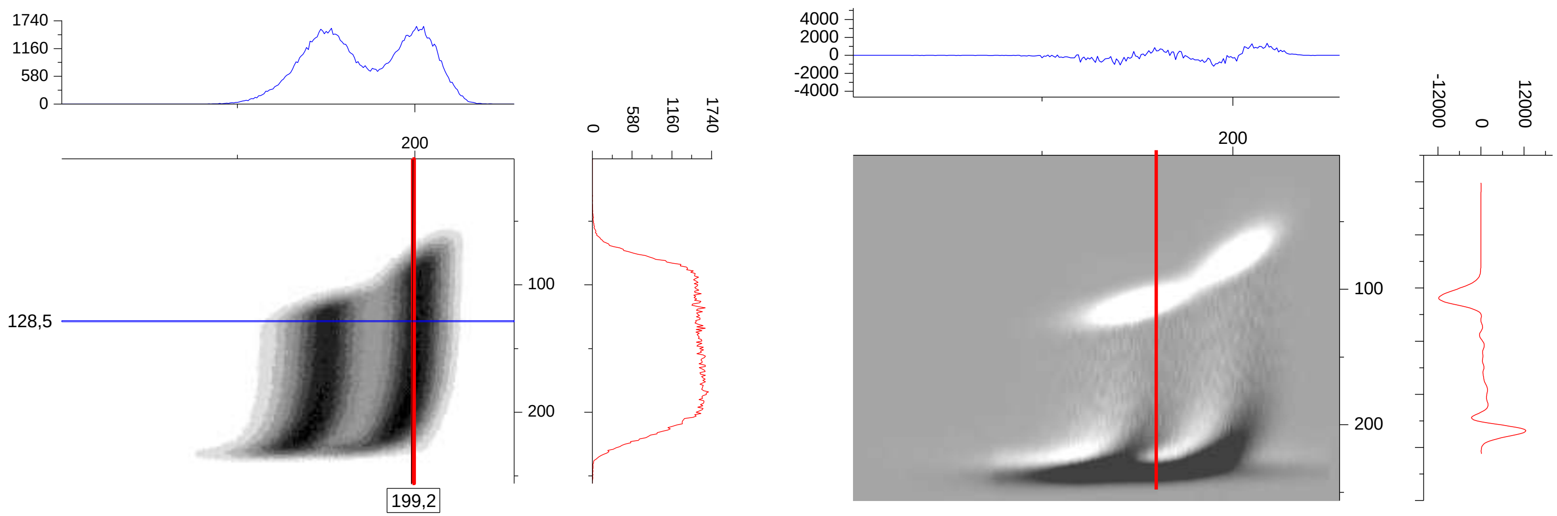

2D plot of pulse height vs drift time P(Q,T)along with profiles to Q-,T-axes(left) . “Partial derivative” $\frac{dP(Q,T)}{DT}$ plotted along with the respective profiles (right). Minimum and maximum on the T-profile corresponds to the 0 and 90 degree angle between FF and the cathode normal respectively

Numerical simulation

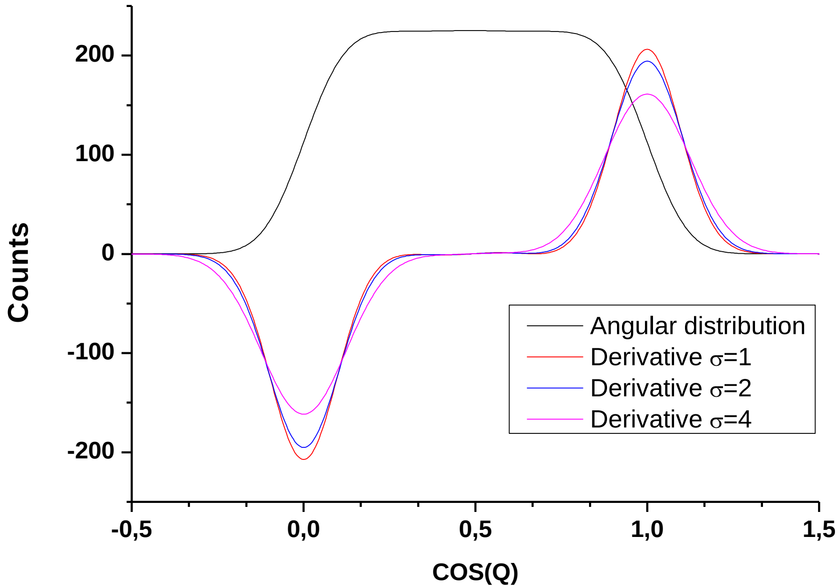

$$F(\mu) = \int_{-\infty}^{\infty} \Pi(\xi) R(\mu - \xi) d\xi$$

$$R(\mu - \xi) = \frac{1}{\sqrt{2\pi\sigma^2}} \exp\left(-\frac{(\mu - \xi)^2}{2\sigma^2}\right)$$

Numerical simulation of rectangular cosine distribution measured with Gaussian response function (black curve). Result of differentiation using Eq. :

$$\int_{-\infty}^{+\infty} \frac{dF(\xi)}{d\xi} R(\mu - \xi) d\xi = F(\xi) R(\mu - \xi)\Big|_{-\infty}^{\infty} - \int_{-\infty}^{\infty} F(\xi) dR(\mu - \xi) = \int_{-\infty}^{\infty} F(\xi) \frac{\mu - \xi}{\sigma^2} R(\mu - \xi) d\xi$$

Real measurement of angular distribution

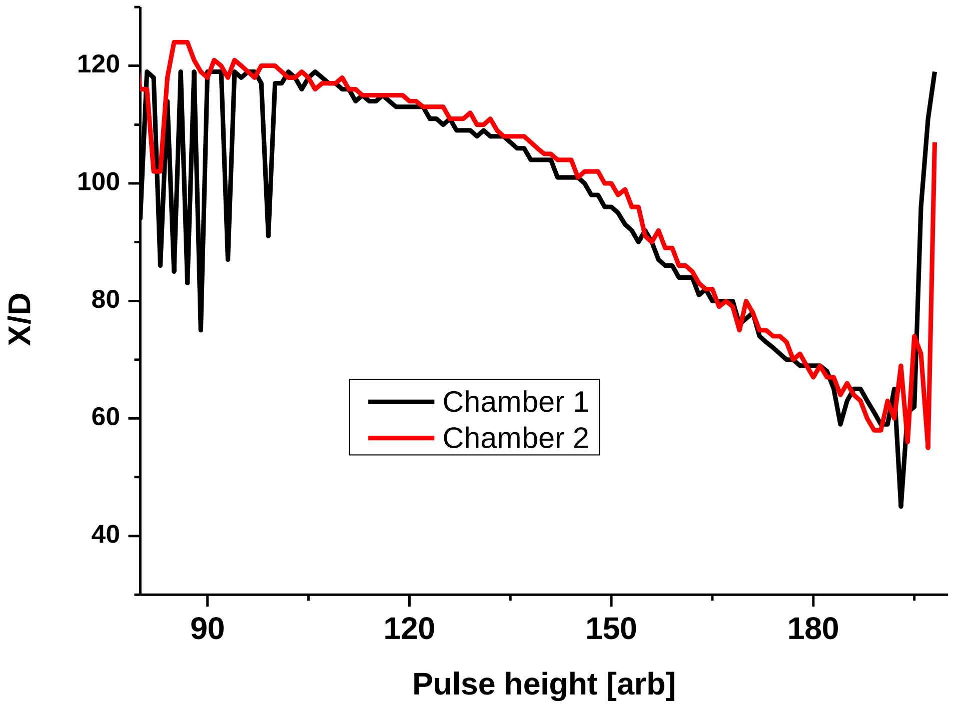

The pulse height dependence of $T_{min}(Q)$~*X* *(the centre of charge distribution along the FF trace)* is plotted in for both halves of the TGIC. For fixed Q (pulse height) the minimum value of drift time realized for FF moving along the normal to the cathode plane. The drift time is maximum for FF at grazing angles.

Comparison of angular distributions

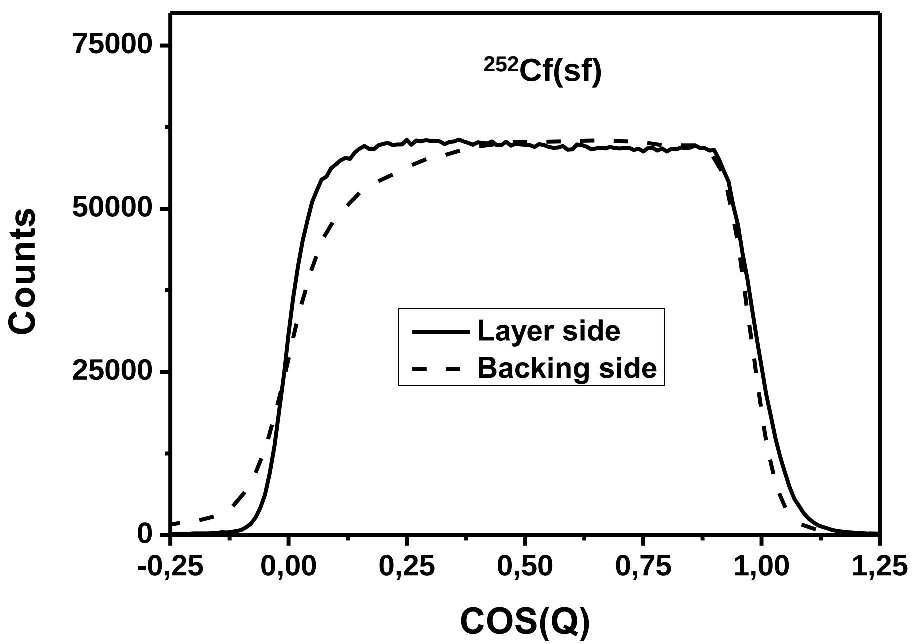

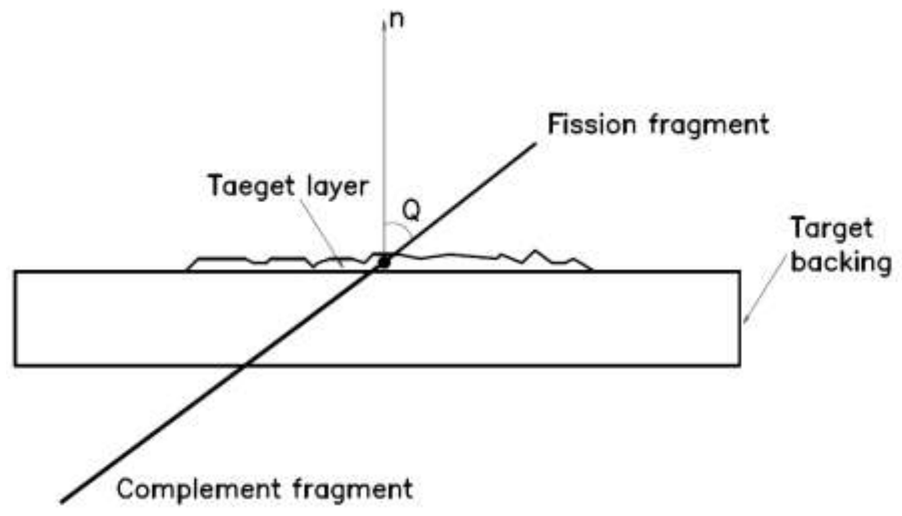

Angular distribution measured from the target layer side demonstrates rather better accuracy, almost independent on the FF angle in respect to the layer surface. The backing side accuracy degrades at FF angle close to 90◦ . This fact makes measurement of PFN emission for targets like ^{235}U and ^{239}Pu very difficult task. To overcome that we developed a position sensitive TIC, allowing measurement with an arbitrary allocated multiple ND

Application: The Stripped Detector

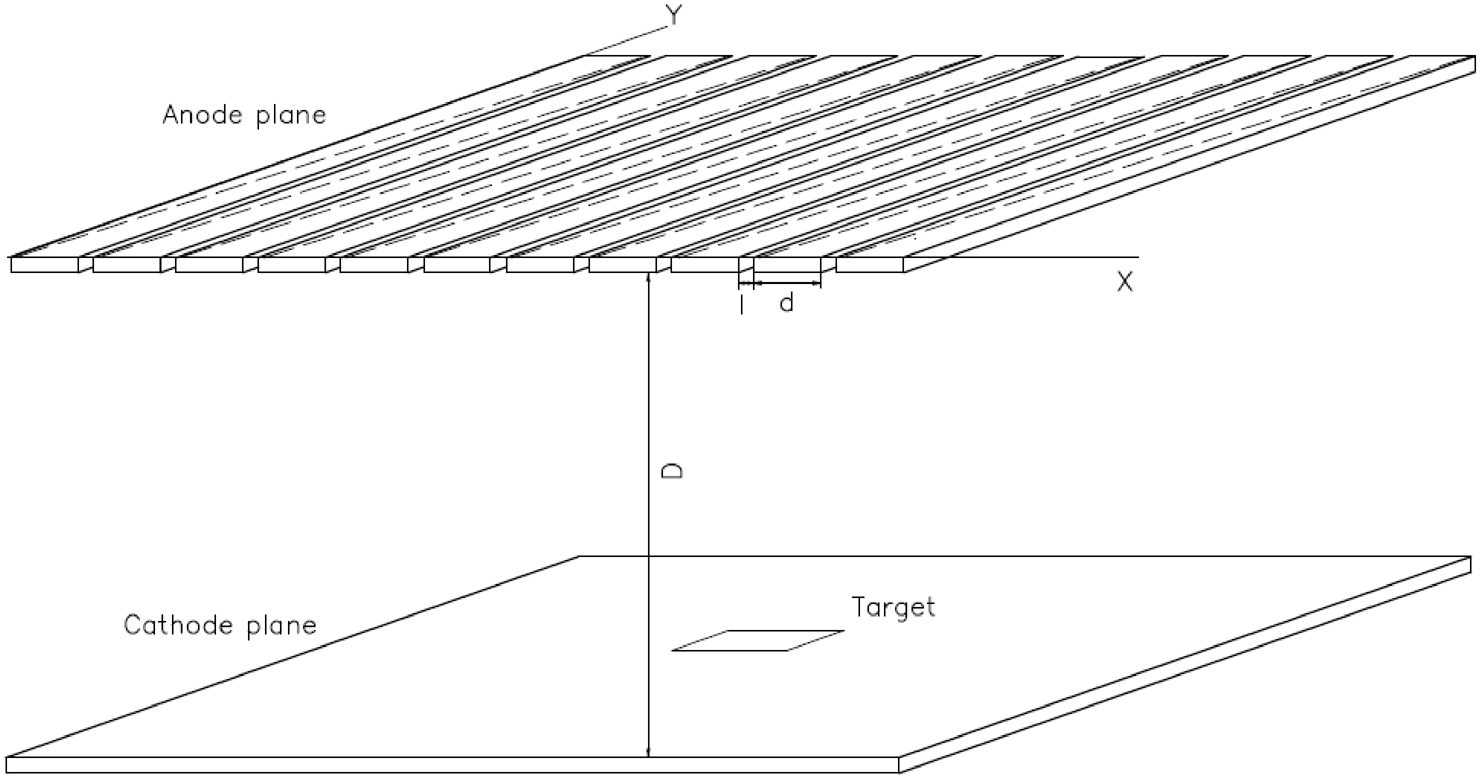

The anode of modified TIC was made of strips and the grid was removed. Strips divided along the diogonal forming two isolated Δ-electrodes. Separate electrical contacts generally are made to each Δ-electrode. No space charges are present in the chamber volume. Dimensions of the chamber in the *x* and y directions are large compared with the thickness of strips, so that edge effects can be neglected .
e

Weighting potential for the single strip

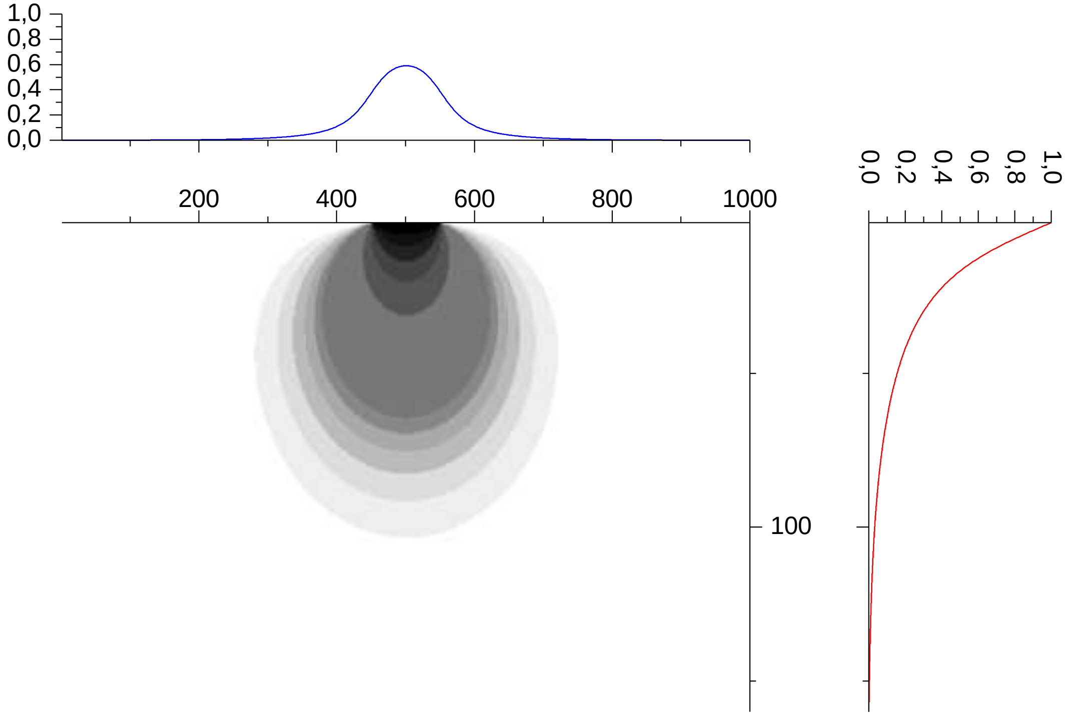

The weighting potential in the TIC volume was calculated for one strip potential raised to 1 leaving other electrodes grounded. If the strips are operated at a positive potential relative to the cathode surface, then electrons will be attracted along field lines that are parallel to each other and perpendicular to the anode surfaces. It is very important to notice that the only electrons that collected by the selected strip will contribute to the pulse formed on the strip circuit.

Comparison with TGIC

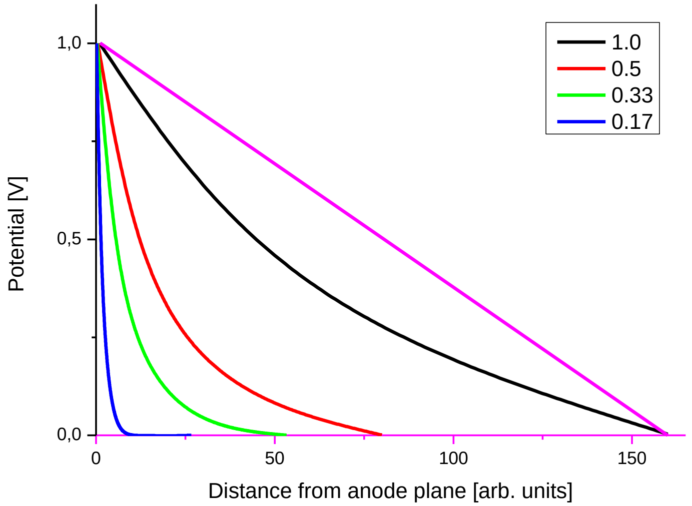

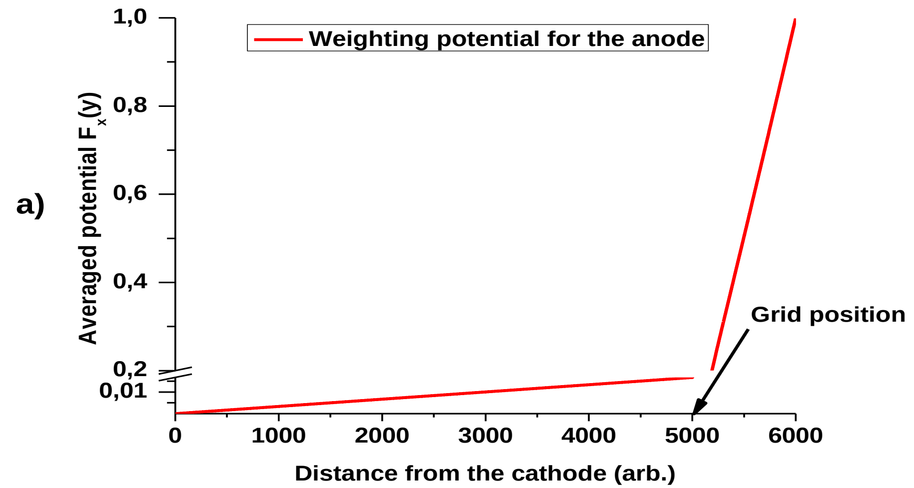

Left graph demonstrates the weighting potential dependence on the ratio of the anode strip width to the anode-cathode distance. On the right graph the weighting potential for the TGIC is shown. Comparison demonstrates that if anode-cathode distance is properly chosen, the there is no need in Frisch-grid at all. This has influence on the pulse shape of individual strip and possibly could facilitate determination of ionization density along the fission fragment deceleration path. This effect was not investigated yet. Another feature of new design is improve of pulse rise time, which makes the TIC more attractive for experiments with targets with high intrinsic alpha-radiation.

Non point target

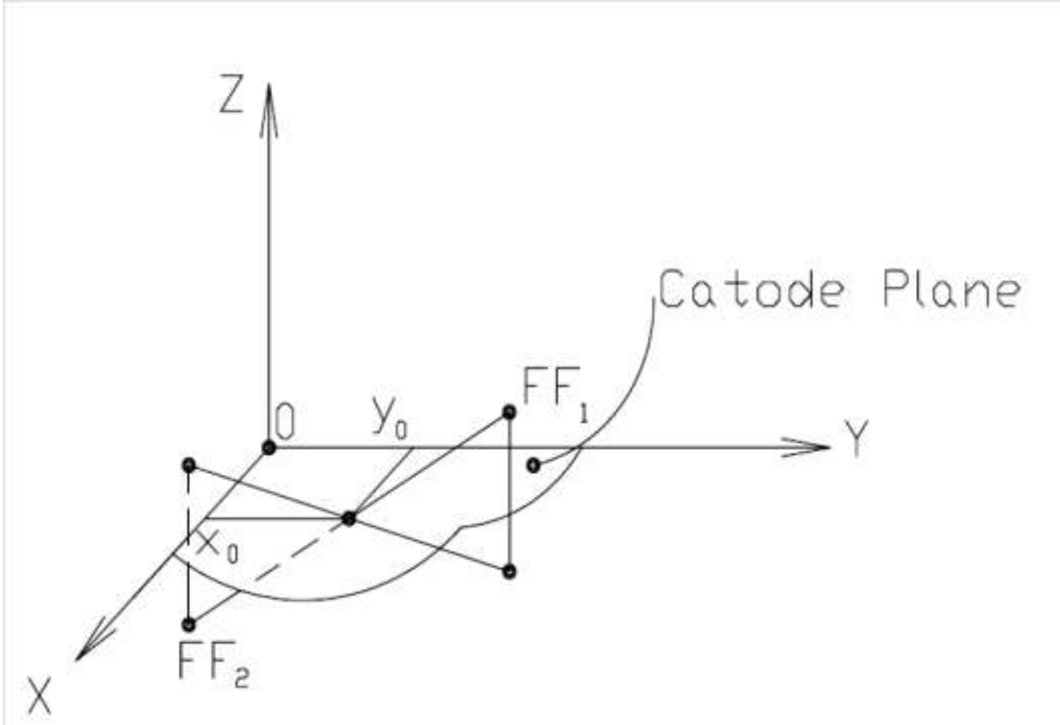

Point target investigation was realized so far only with ^{252}Cf nucleus. For the majority of interesting nuclei point target option is not available for different reasons, but instead large area thin targets (100-200 sq. cm with thickness of 40-60 μG/sq. cm) can be manufactured. PFN investigation is difficult due to small cross section of fission reactions. One of the way to overcome that difficulty is to use large area target and as much as possible the number of ND. Then the task of reaction kinematics reconstruction can be solved by the position sensitive TIC measuring FF angles in 3D Cartesian coordinates

FF angle determination in 3D Cartesian coordinates

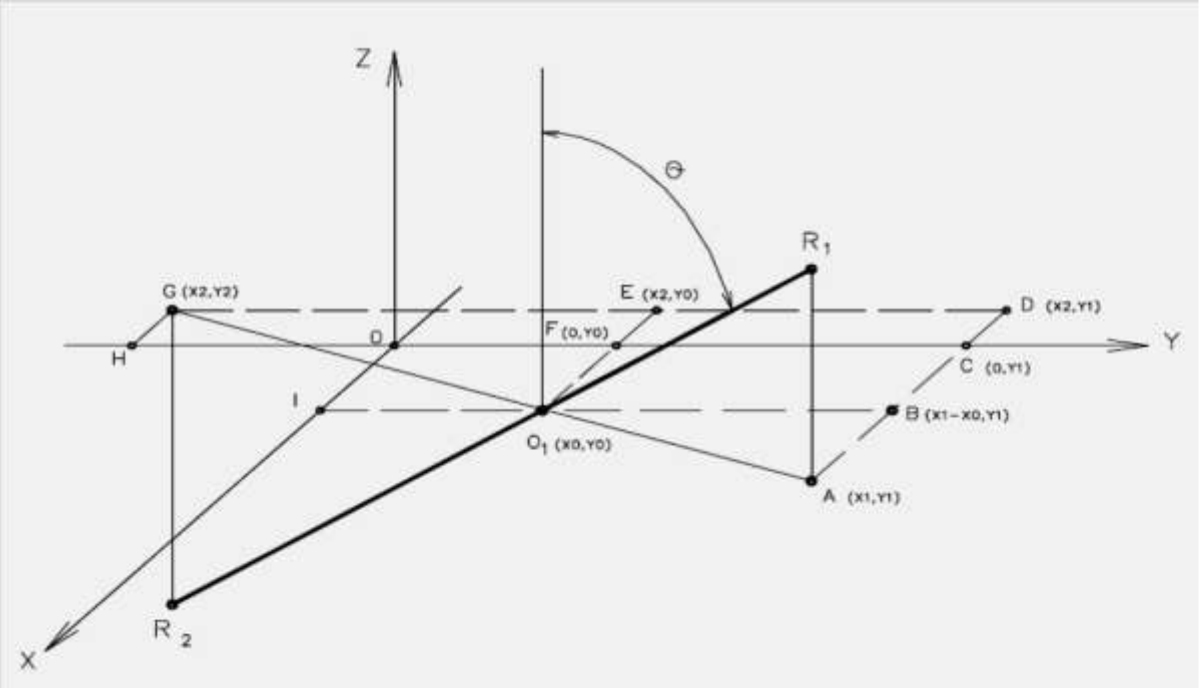

$$\frac{x_1 - x_0}{x_1 + x_2} = \frac{R_1}{R_1 + R_2} \Rightarrow x' = x_1 - x_0 = (x_1 + x_2)\frac{R_1}{R_1 + R_2} \qquad \frac{x_2 + x_0}{x_1 + x_2} = \frac{R_2}{R_1 + R_2} \Rightarrow x' = x_2 + x_0 = (x_1 + x_2)\frac{R_2}{R_1 + R_2}$$

$$\frac{y_1 - y_0}{y_1 + y_2} = \frac{R_1}{R_1 + R_2} \Rightarrow y' = y_1 - y_0 = (y_1 + y_2)\frac{R_1}{R_1 + R_2} \qquad \frac{y_2 + y_0}{y_1 + y_2} = \frac{R_2}{R_1 + R_2} \Rightarrow y' = y_2 + y_0 = (y_1 + y_2)\frac{R_2}{R_1 + R_2}$$

$$COS(X) = \frac{x_1 + x_2}{R_1 + R_2}; \quad \mathrm{COS(X)} = \frac{\mathrm{x}_2 + \mathrm{x}_0}{R_2}; \mathrm{COS(Y)} = \frac{y_1 + y_2}{R_1 + R_2}; \quad \mathrm{COS(Y)} = \frac{\mathrm{y}_2 + \mathrm{y}_0}{R_2};$$

Unfolding of angular distributions

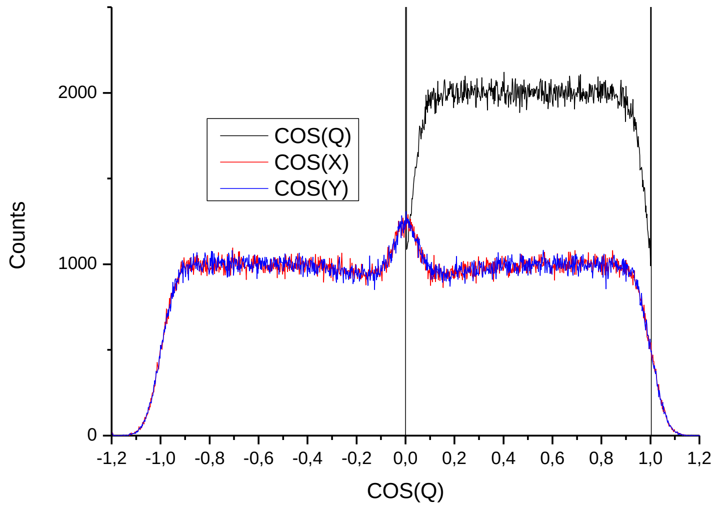

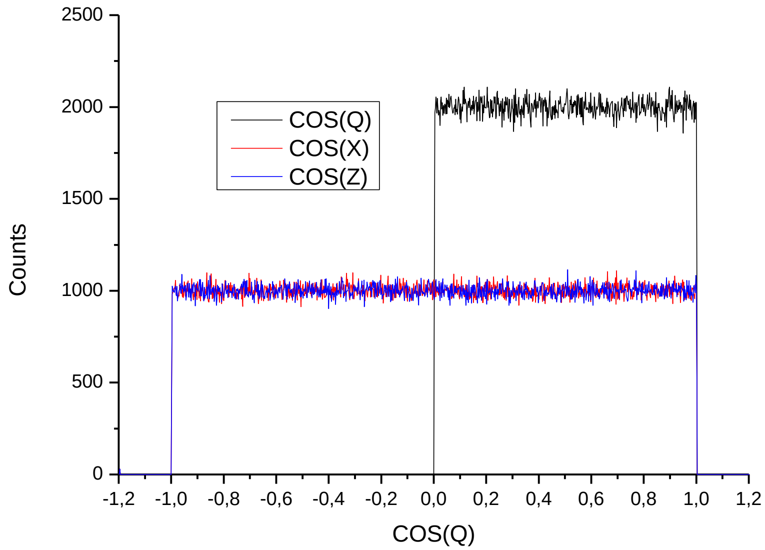

Unfolding procedure is illustrated by two figures above. First graph illustrates COS(X) and COS(Y) values Calculated from the row data truncated according to the following formula: if COS(Q)>1 then COS(Q)=1.

On the right side graph the unfolded angular distribution functions are presented. The idea of unfolding came from the Shannon sampling theorem. According to the theorem: continuous function can be represented by its sampled form periodically expanded over the argument. Using this the unfolding of angular distribution can be reduced to the following simple formula:

if(COS(Q) > 1) then D=1-COS(Q) COS(Q)unf= 1-D;

Result of such unfolding procedure is presented on the right side graph.

Average PFN number versus FF mass in comparison with previous measurements

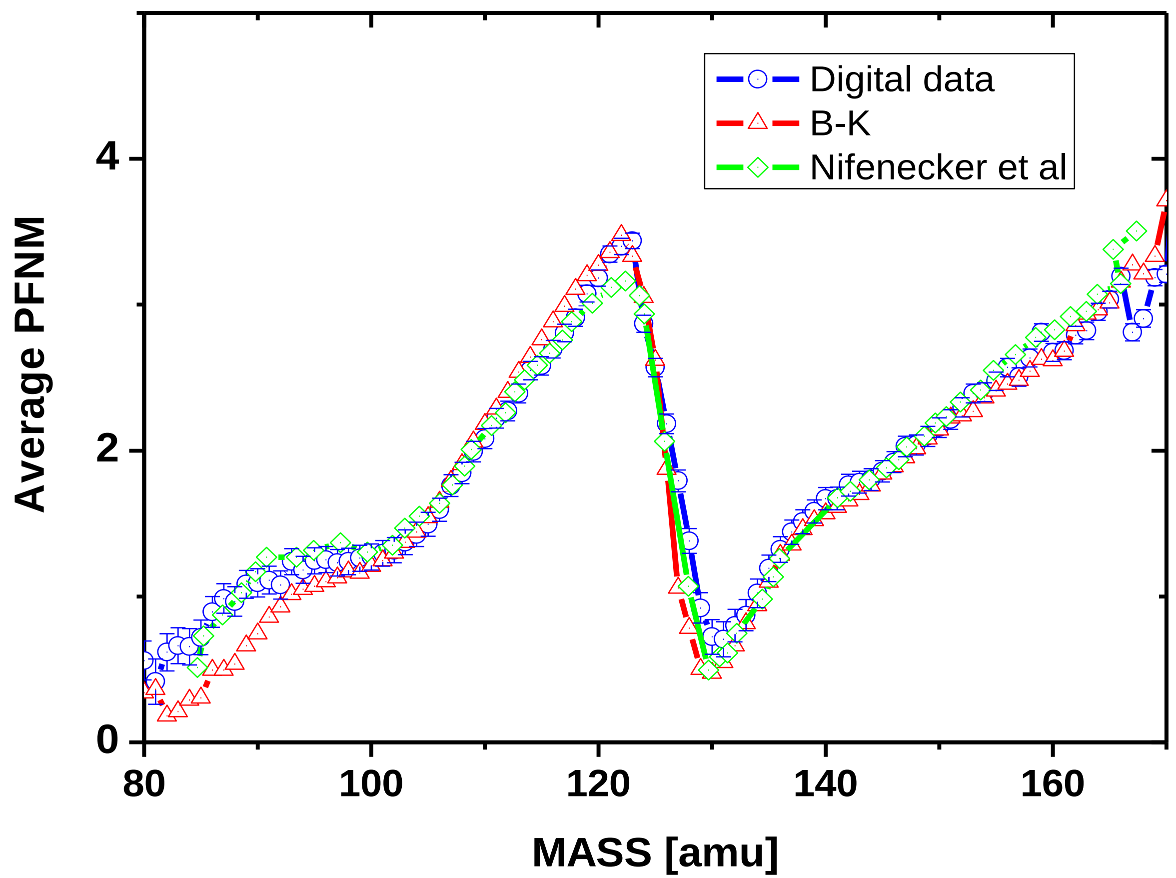

$$\bar{\nu}(A) = \frac{\int_0^\infty \bar{\nu}(A,TKE)Y(A,TKE)dTKE}{\int_0^\infty Y(A,TKE)dTKE}, \quad \bar{\nu} = \int_0^\infty \bar{\nu}(A,TKE)Y(A,TKE)dTKE\,dA, \quad 200 = \int_0^\infty Y(A,TKE)dTKE\,dA$$

Average PFN number versus TKE in comparison with literature

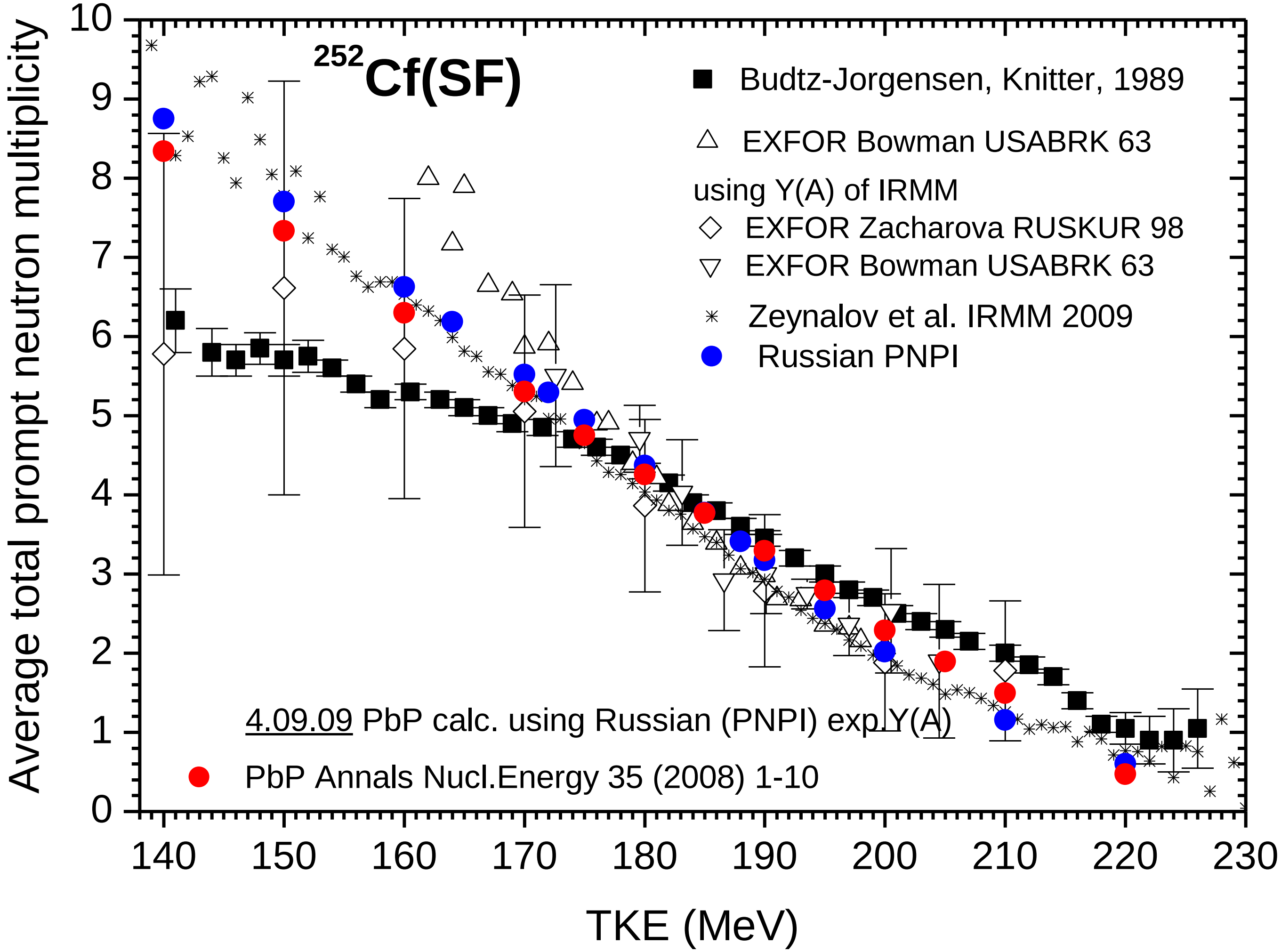

$$\bar{\nu}(TKE) = \frac{\int_0^\infty \bar{\nu}(A,TKE)Y(A,TKE)dA}{\int_0^\infty Y(A,TKE)dA}, \quad \bar{\nu} = \int_0^\infty \bar{\nu}(A,TKE)Y(A,TKE)dTKEdA, \quad 200 = \int_0^\infty Y(A,TKE)dTKEdA$$

Average PFN number versus TKE for selected FF mass numbers

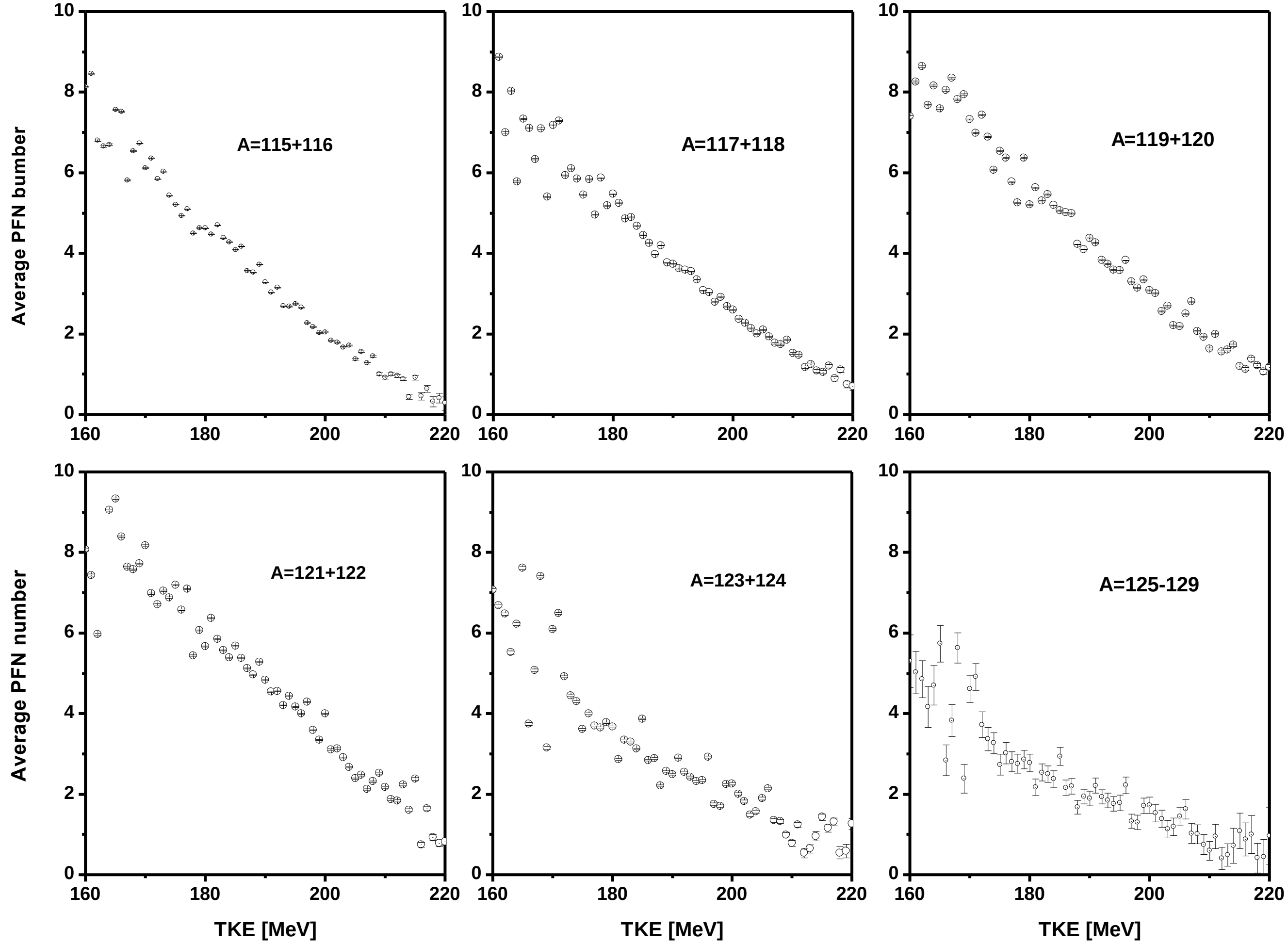

$$\bar{\nu}(TKE)\big|_A = \frac{\bar{\nu}(A,TKE)Y(A,TKE)}{Y(A,TKE)}, \quad \bar{\nu} = \int_0^{\infty} \bar{\nu}(A,TKE)Y(A,TKE)dTKEdA, \quad 200 = \int_0^{\infty} Y(A,TKE)dTKEdA$$

Neutron imaging with n-γ converter and CCD camera

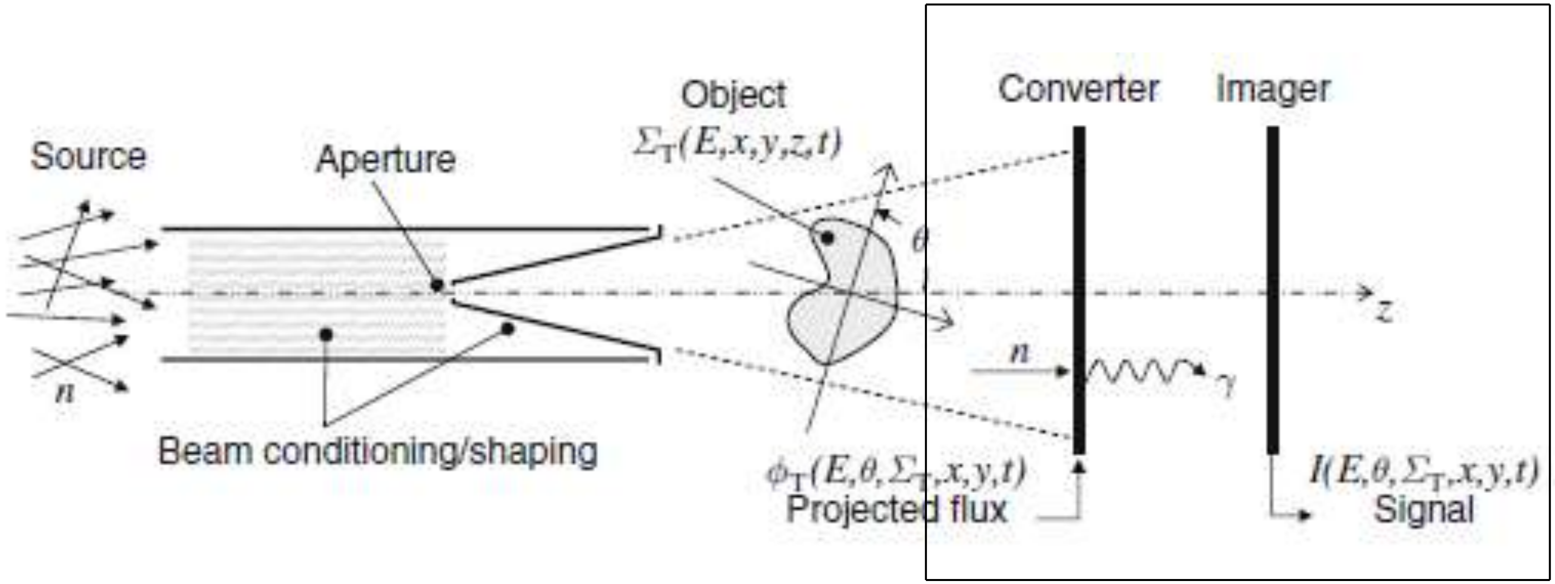

Summary and conclusions

Significant modifications of the experimental methods were done in our work thanks to flexibility and power provided by the digital signal processing .

Many conclusions of previous investigations have been confirmed in our work. At the same time we managed to resolve the longstanding contradiction between experimental results and theoretical calculations. With higher confidence than in previous investigations we proved the statement on isotropic PFN emission in FF's centre-of-mass reference frame.

For the first time it was shown that dependence of average PFN multiplicity is linear as was expected from the theory. This made obsolete experiments, where search of pre-scission neutrons was expected to resolve the problem of PFN deficit at low TKE values.

We developed new fission detector and advanced mathematical data analysis, which we believe opens a new perspective in study of PFN emission in low energy fission.

A new detector can be used in neutron imaging applications as a competitive option to existing solutions.

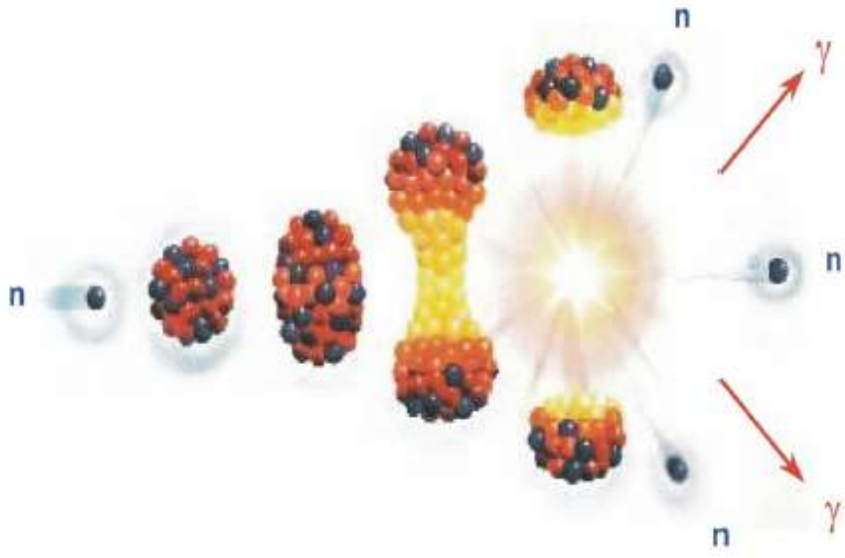

Thank you for your attention ☺